Supplement of Hydrol. Earth Syst. Sci., 30, 779–795, 2026
https://doi.org/10.5194/hess-30-779-2026-supplement

Hydrology and Earth System Sciences
Open Access

Supplement of

Uncertainty, temporal variability, and influencing factors of empirical streamflow sensitivities

Sebastian Gnann et al.

Correspondence to: Sebastian Gnann (sebastian.gnann@hydrologie.uni-freiburg.de)

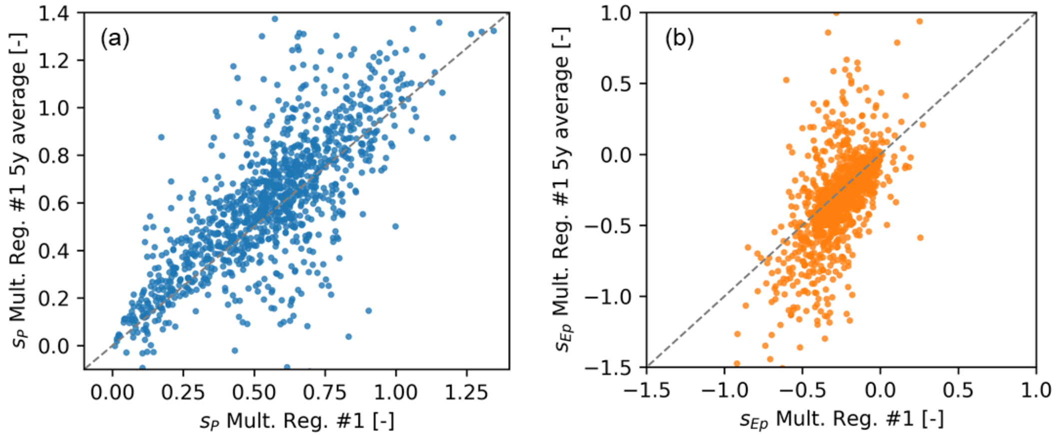

Figure S1: Comparison between estimated sensitivities using annual averages of P and E_p and estimated sensitivities using averages over non-overlapping 5-year blocks, both estimated using Multiple Regression #1. Panel (a) shows streamflow sensitivity to precipitation (Spearman correlation $\rho_s = 0.74$) and panel (b) shows streamflow sensitivity to potential evaporation ($\rho_s = 0.65$). The results broadly agree, though the sensitivities estimated using 5-year averages fall more often outside the theoretical range (e.g., $s_P > 1$ or $s_{Ep} > 0$).

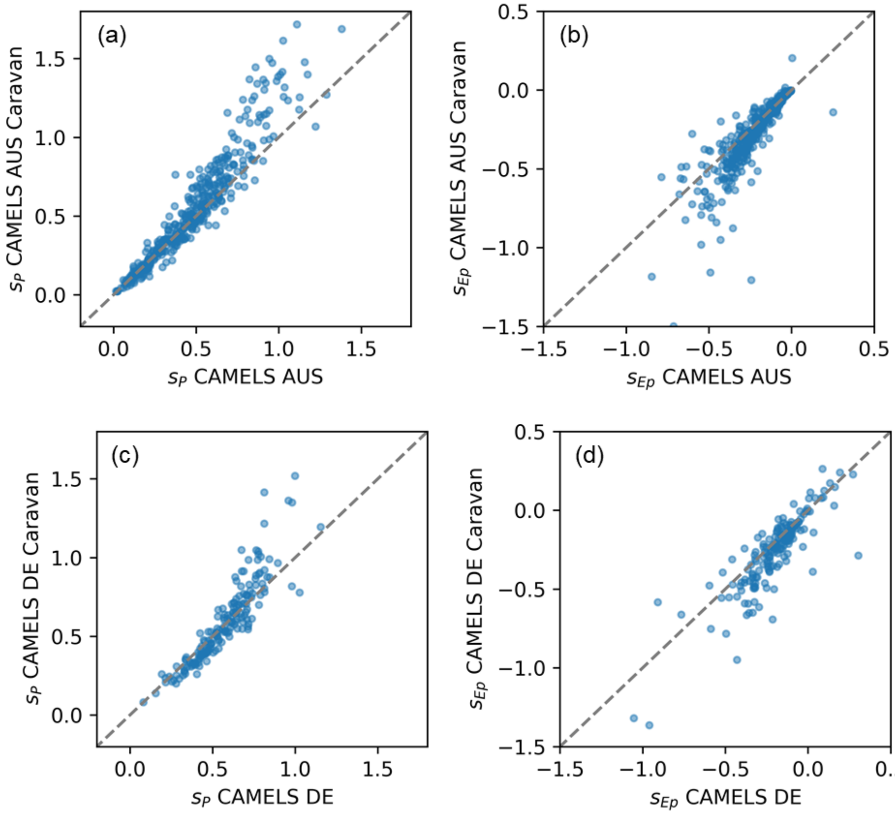

Figure S2: Comparison between sensitivities derived from national forcing products and Caravan forcing for (a) streamflow sensitivity to precipitation for CAMELS-AUS v2 (ρ_s = 0.97), (b) streamflow sensitivity to potential evaporation for CAMELS-AUS v2 (ρ_s = 0.94), (c) streamflow sensitivity to precipitation for CAMELS-DE (ρ_s = 0.94), and (d) streamflow sensitivity to potential evaporation for CAMELS-DE (ρ_s = 0.86).

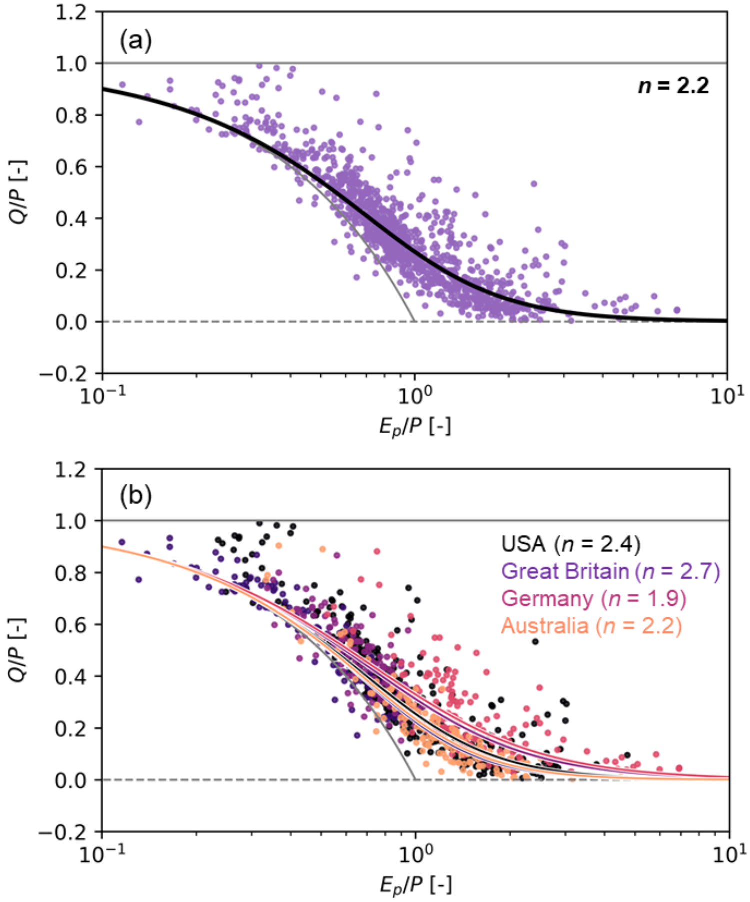

Figure S3: Budyko plots showing the Turc-Mezentsev model alongside the 1121 catchments analysed in the corresponding manuscript, with (a) the parameter *n* being calibrated to the entire dataset and (b) the parameter *n* being calibrated to each national dataset individually.

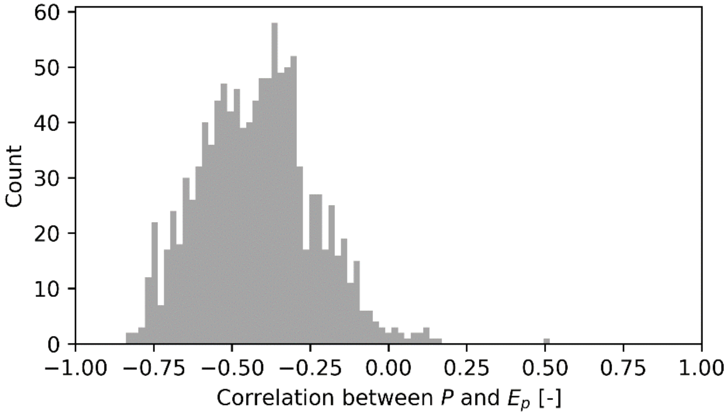

Figure S4: Pearson correlation ρ_p between precipitation and potential evaporation for the entire dataset (average = -0.42). Overall, 16 catchments (located in the US, Great Britain, and Germany) show a positive correlation between precipitation and potential evaporation.

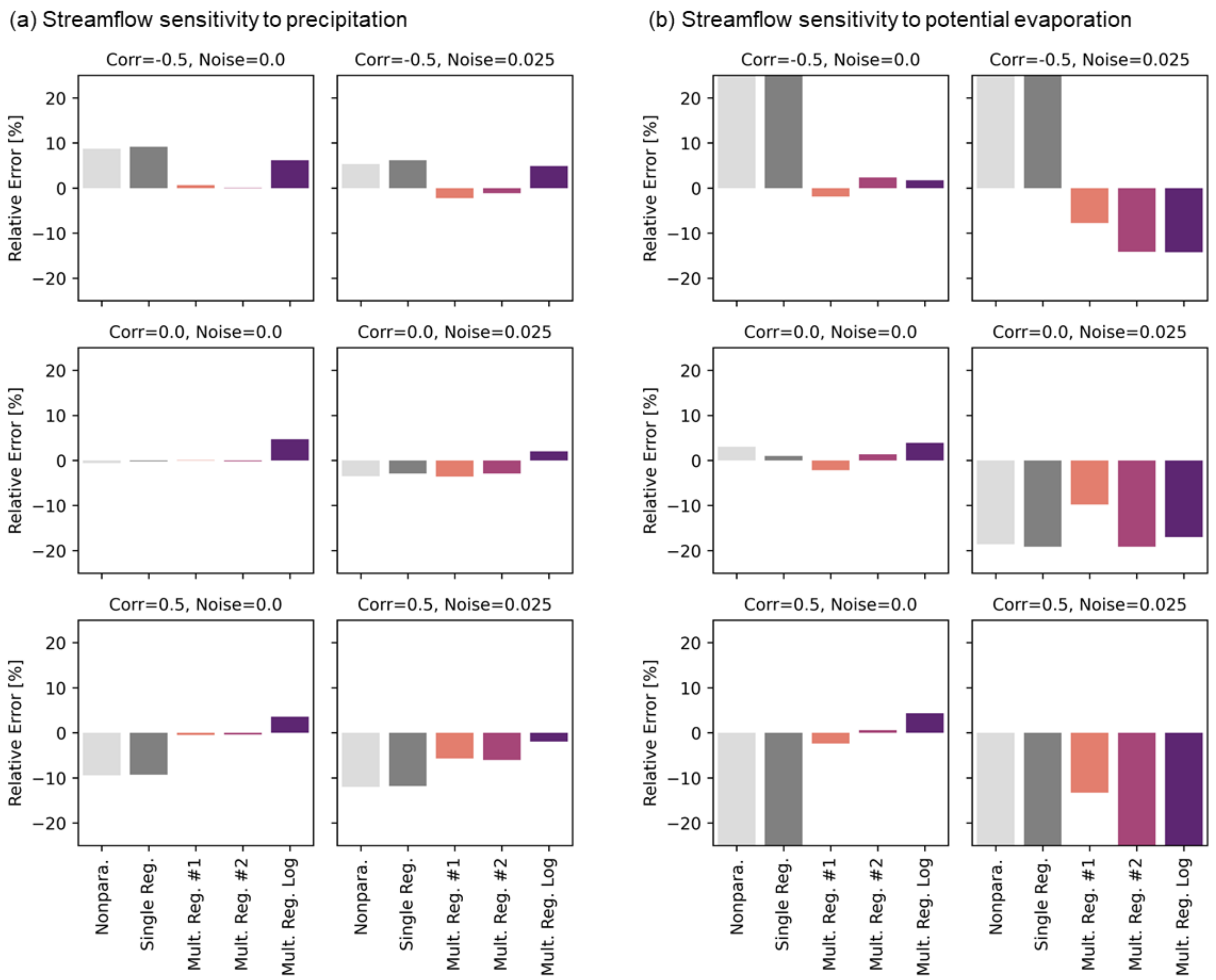

Figure S5: Average relative errors for the different estimation methods when applied to synthetic data with different degrees of correlation and noise. (a) Streamflow sensitivity to precipitation. (b) Streamflow sensitivity to potential evaporation. Note that the y-axes are capped for better visibility.

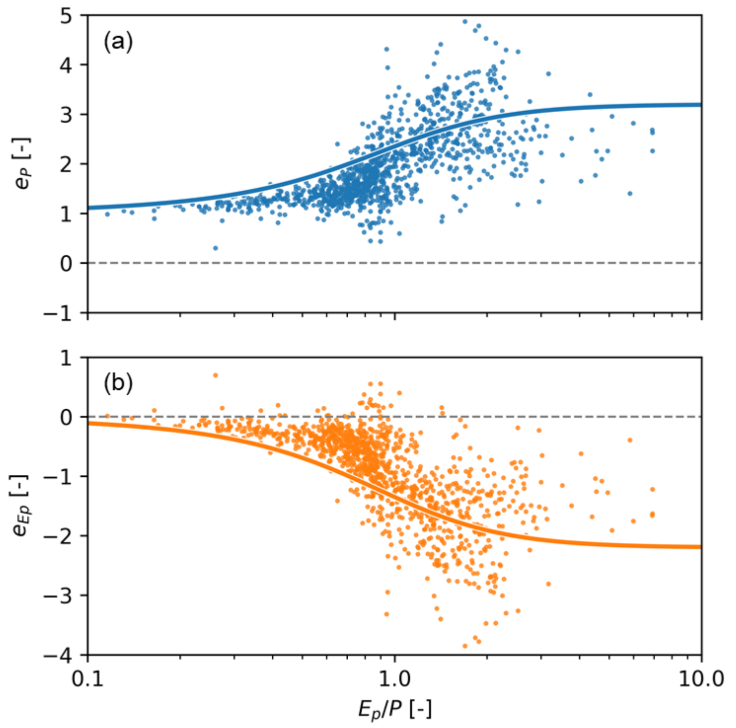

Figure S6: Streamflow elasticity to (a) precipitation and (b) potential evaporation, calculated using multiple regression #1 with observations from 1121 catchments. Both panels show empirically calculated values (dots) and theoretical values based on the Turc-Mezentsev model with n = 2.2 (solid lines). Note that the y-axes are capped for better visibility.

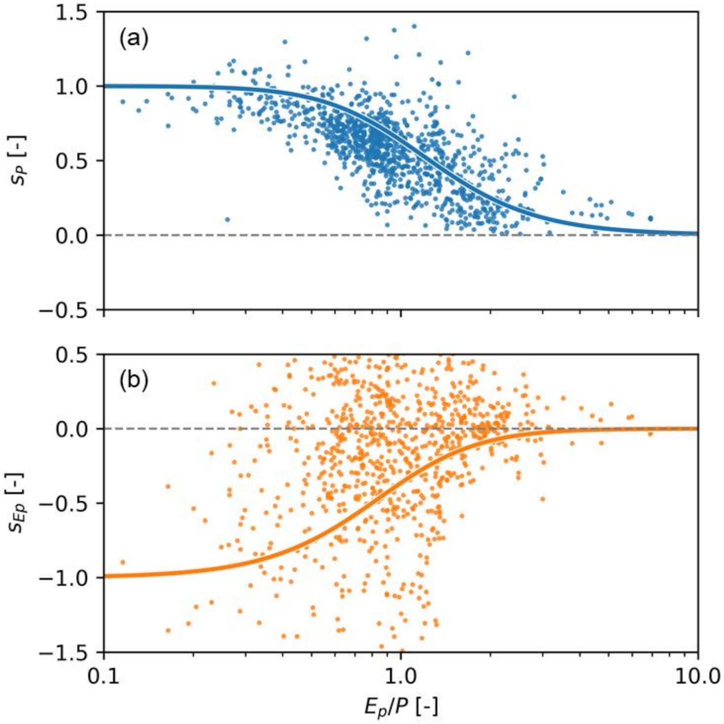

Figure S7: Streamflow sensitivity to (a) precipitation and (b) potential evaporation, calculated using multiple regression #2 with observations from 1121 catchments. Both panels show empirically calculated values (dots) and theoretical values based on the Turc-Mezentsev model with $n = 2.2$ (solid lines). Note that the y-axes are capped for better visibility and thus not all catchments are shown.

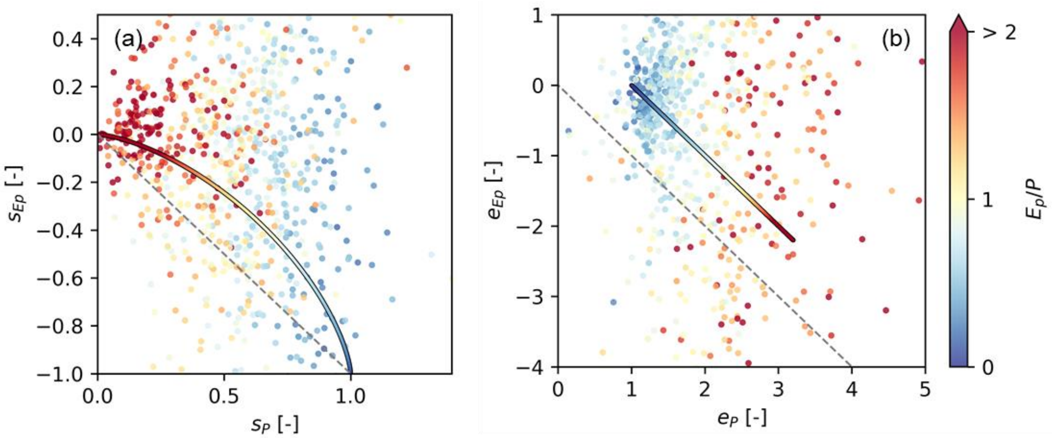

Figure S8: (a) Streamflow sensitivity to precipitation plotted against streamflow sensitivity to potential evaporation. (b) Streamflow elasticity to precipitation plotted against streamflow elasticity to potential evaporation. Both panels show empirically calculated values using multiple regression #2 (dots in the back) and theoretical values based on the Turc-Mezentsev model (line in front), coloured according to the aridity index. The grey dashed line starts at the origin and has a slope of -1, so that values plotting above it imply that $s_P > s_{Ep}$ (a) and $e_P > e_{Ep}$ (b).

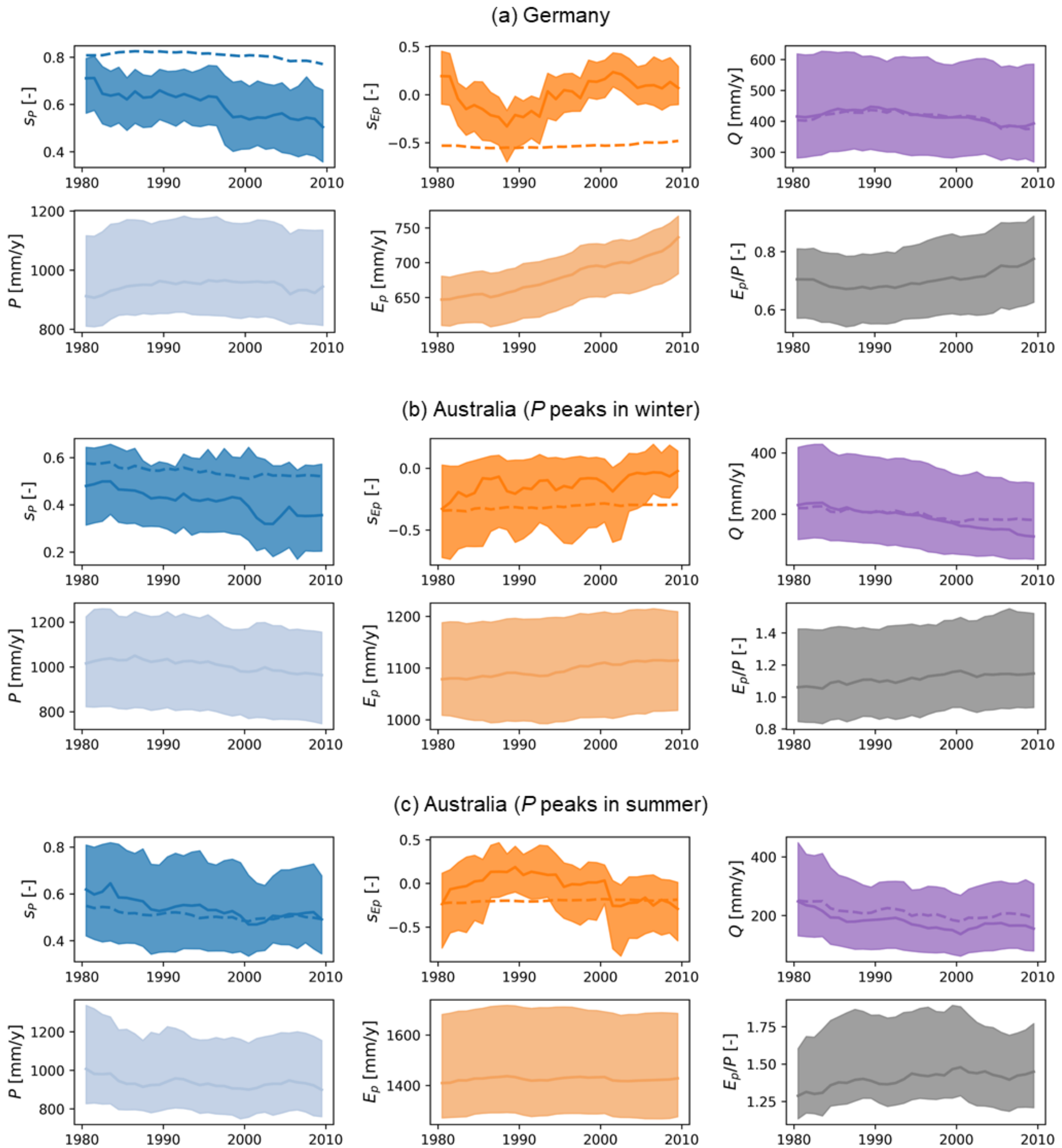

Figure 9: Change of streamflow sensitivities and other variables over time for (a) 144 catchments in Germany, (b) 100 catchments in Australia with most precipitation falling in winter ($P_S < 0$), and (c) 109 catchments in Australia with most precipitation falling in summer ($P_S > 0$). Shaded areas indicate the 25th and 75th percentiles and thick lines indicate the median of all catchments Dashed lines indicate the trends calculated with the Turc-Mezentsev model for the sensitivities and Q based on observed P and E_p data and using a calibrated value of n = 1.9 for (a), n = 1.7 for (b) and n = 2.6 for (c). Sensitivities are calculated using method #1 over 20-year blocks with the middle year shown (e.g., 1980 indicates a block from 1970 to 1990).

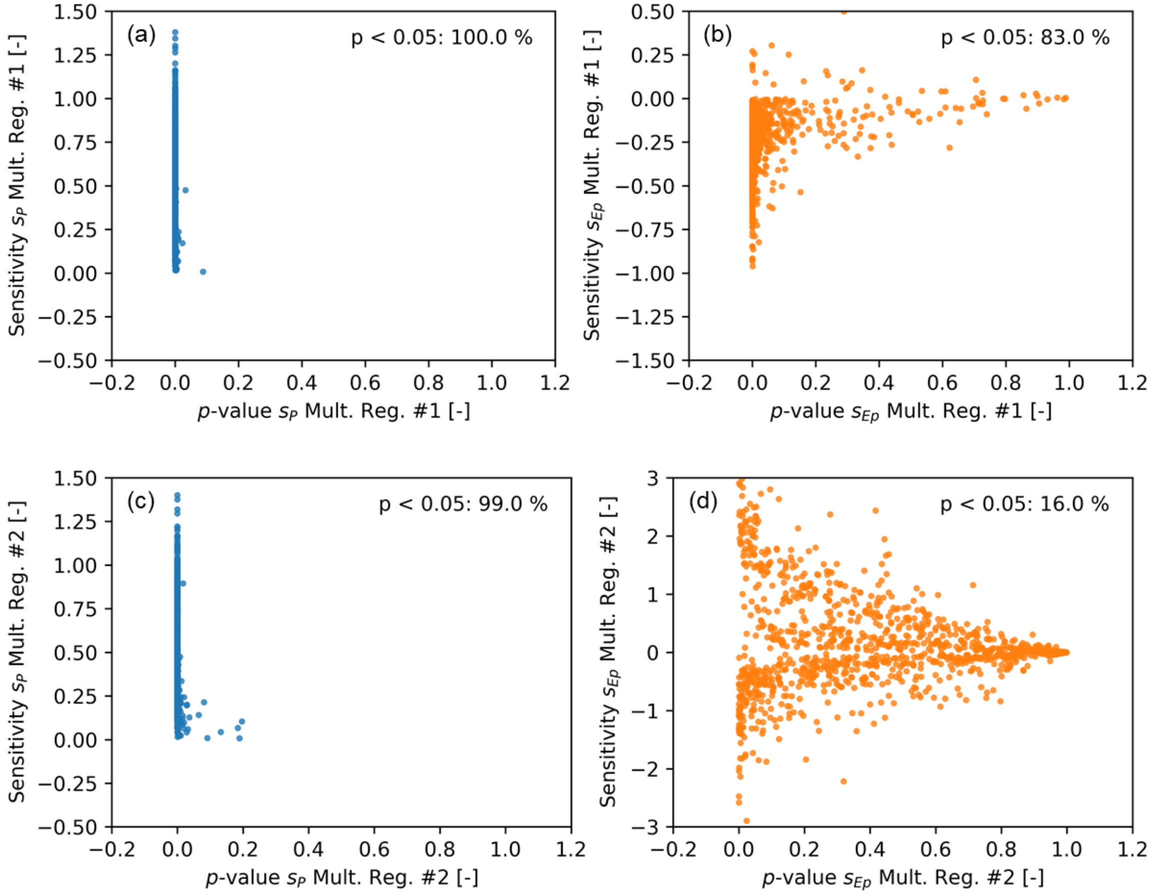

Figure S10: Scatter plot showing *p*-values against their regression coefficients (i.e., sensitivities) for multiple regression methods #1 (a, b) and #2 (c, d).

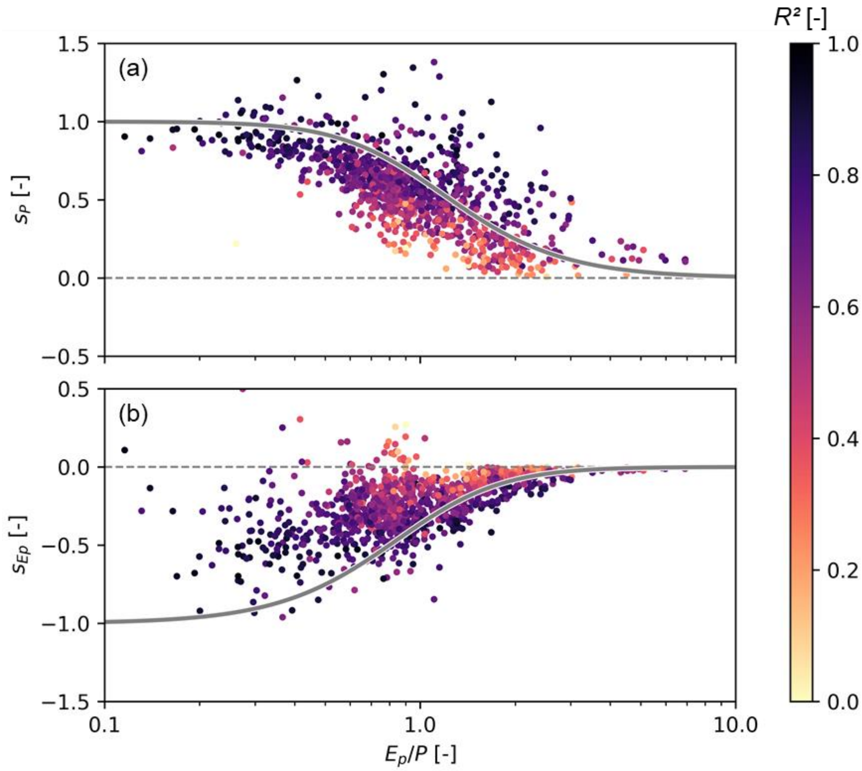

Figure S11: Streamflow sensitivity to precipitation (a) and potential evaporation (b) calculated using multiple regression method #1 with observations from 1121 catchments, coloured according to R^2. Both panels show empirically calculated values (dots) and theoretical values based on the Turc-Mezentsev model (dashed lines). Note that the y-axes are capped for better visibility. Spearman rank correlation ρ_S between R^2 and relative deviation from the Turc-Mezentsev curve is 0.60 for s_P and 0.25 for s_{Ep}.

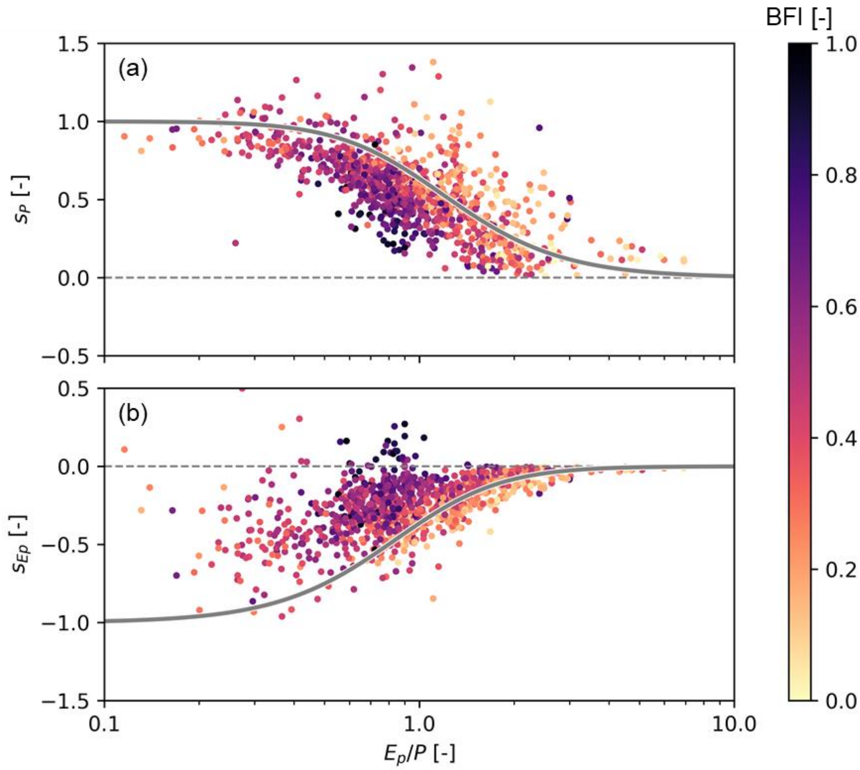

Figure S12: Streamflow sensitivity to precipitation (a) and potential evaporation (b) calculated using multiple regression method #1 with observations from 1121 catchments, coloured according to the baseflow index (BFI). Both panels show empirically calculated values (dots) and theoretical values based on the Turc-Mezentsev model (dashed lines). Note that the y-axes are capped for better visibility. Spearman rank correlation ρ_S between BFI and relative deviation from the Turc-Mezentsev curve is -0.41 for s_P and -0.44 for s_{Ep}.

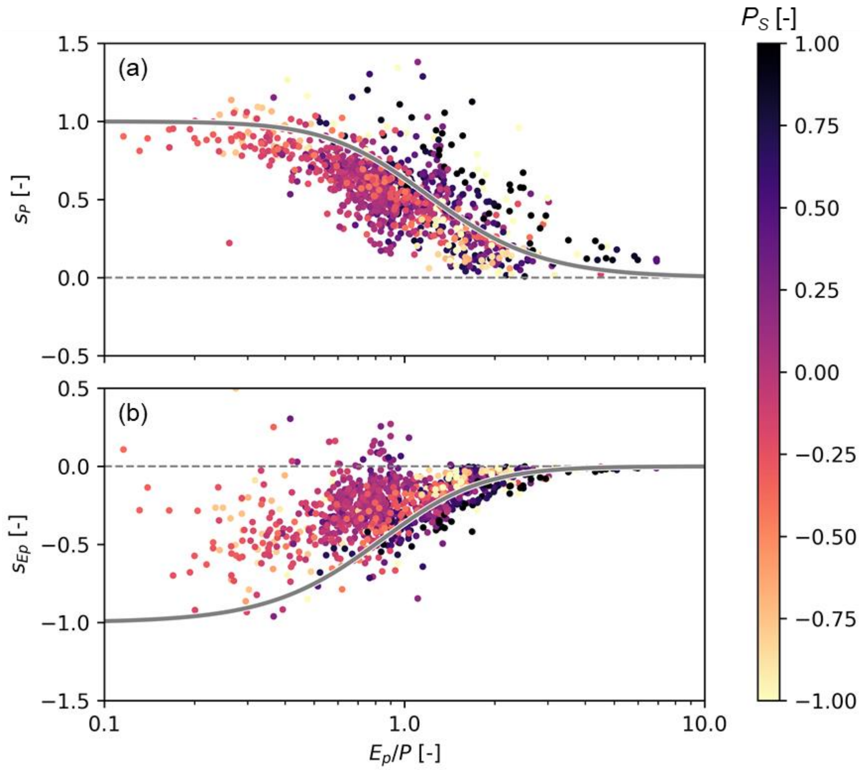

Figure S13: Streamflow sensitivity to precipitation (a) and potential evaporation (b) calculated using multiple regression method #1 with observations from 1121 catchments, coloured according to precipitation seasonality P_S. Both panels show empirically calculated values (dots) and theoretical values based on the Turc-Mezentsev model (dashed lines). Note that the y-axes and the colour scale are capped for better visibility. Spearman rank correlation ρ_S between P_S and relative deviation from the Turc-Mezentsev curve is 0.09 for s_P and 0.20 for s_{Ep}.

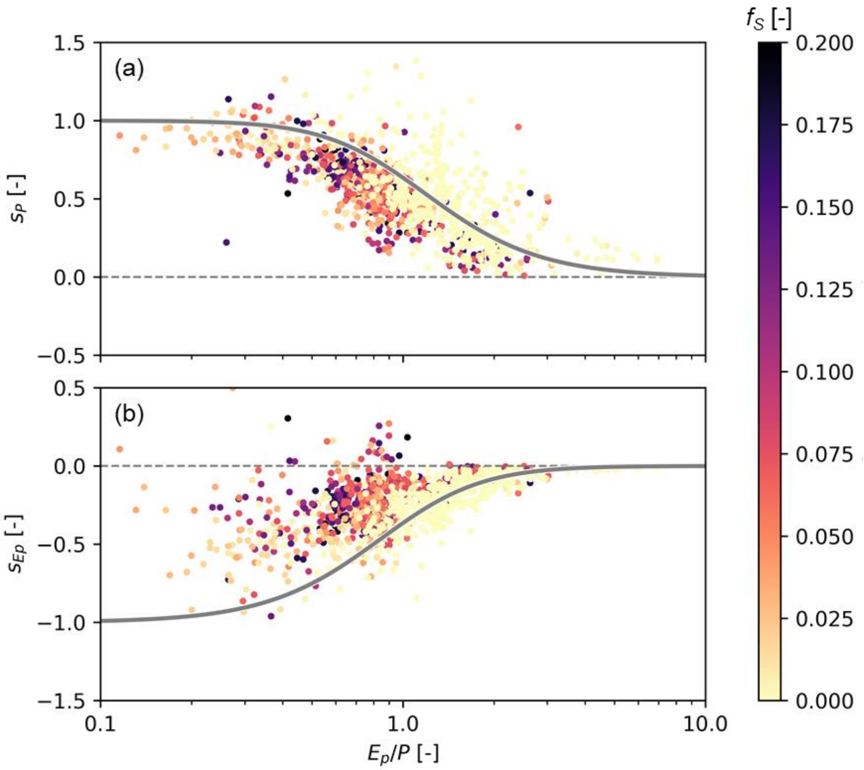

Figure S14: Streamflow sensitivity to precipitation (a) and potential evaporation (b) calculated using multiple regression method #1 with observations from 1121 catchments, coloured according to snow fraction f_S. Both panels show empirically calculated values (dots) and theoretical values based on the Turc-Mezentsev model (dashed lines). Note that the y-axes are capped for better visibility. Spearman rank correlation f_S between P_S and relative deviation from the Turc-Mezentsev curve is -0.31 for s_P and -0.46 for s_{Ep}.

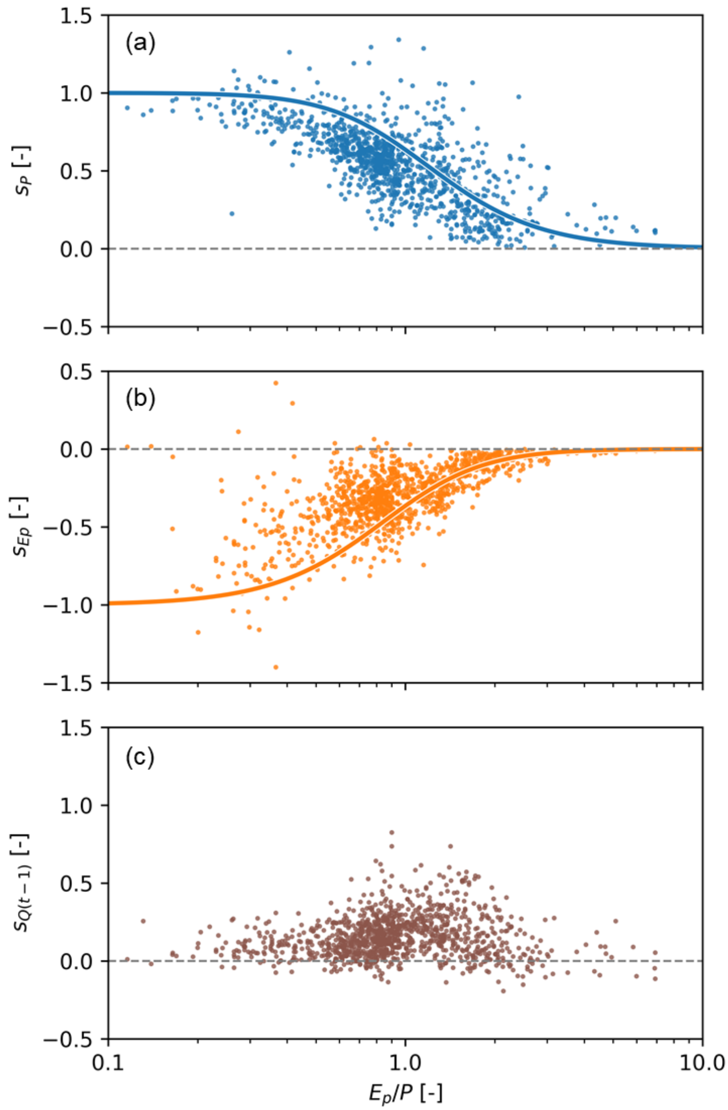

Figure S15: Streamflow sensitivity to precipitation s_P (a), potential evaporation s_{Ep} (b), and (c) storage $s_{Q(t\text{-}1)}$ (using previous year's streamflow $Q(t\text{-}1)$ as a proxy), calculated using multiple regression method #1 with observations from 1121 catchments, but now with an additional storage predictor. Both panels show empirically calculated values (dots) and theoretical values based on the Turc-Mezentsev model (dashed lines). Note that the y-axes are capped for better visibility. The median R^2 for the storage model leads to a slight improvement from 0.65 to 0.69, suggesting that it can explain a larger proportion of the variation in the data, while the values for s_P and s_{Ep} remain relatively stable.

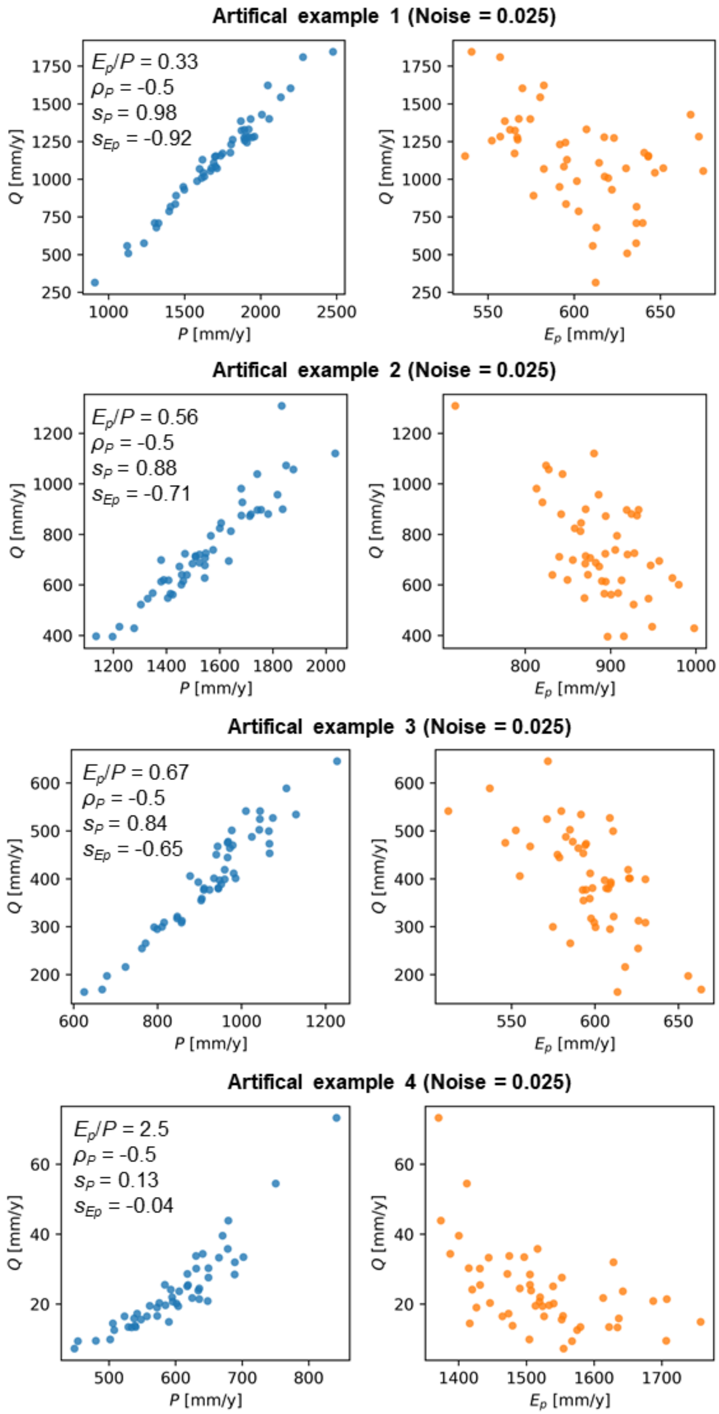

Figure S16: Scatter plots showing P vs. Q and E_p versus Q of 4 artificial catchments created using the Turc-Mezentsev model (with noise and a correlation between P and E_p of -0.5), as well as the corresponding sensitivities. The catchments are ordered based on the aridity index.

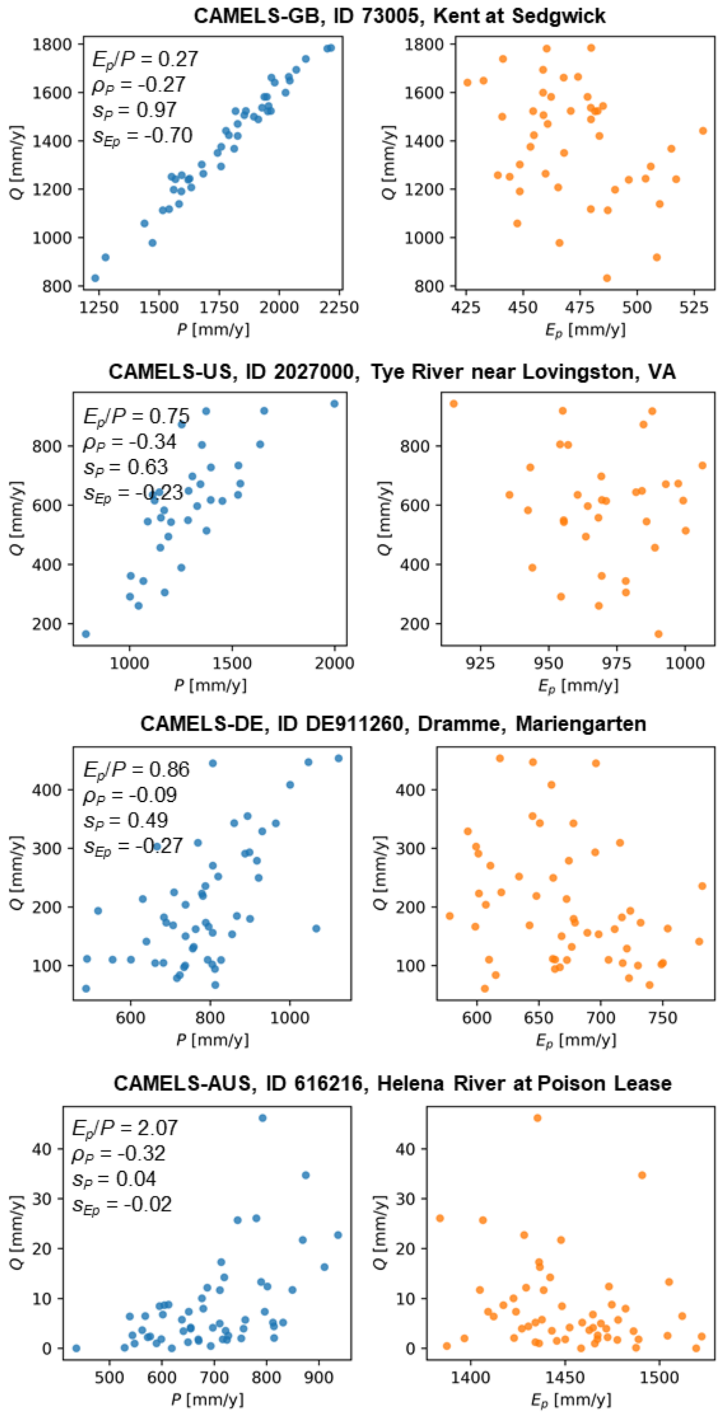

Figure S17: Scatter plots showing P versus Q and E_p versus Q of 4 catchments, as well as the corresponding correlation between P and E_p and the sensitivities, estimated using Multiple Regression #1. The catchments are ordered based on the aridity index.

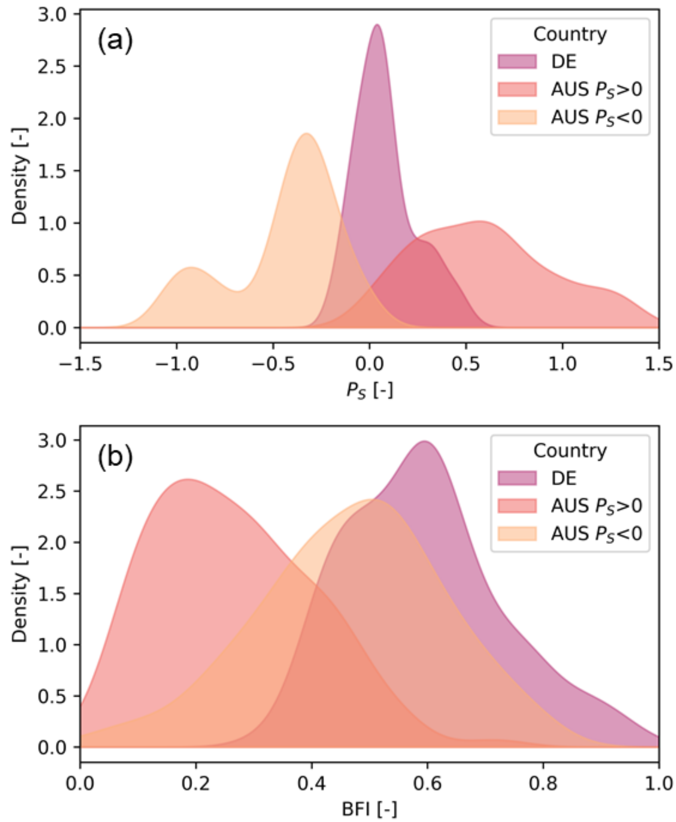

Figure S18: Distributions of precipitation seasonality (a) and baseflow index (b) based on a Gaussian kernel density (KDE) estimation for the German catchments and the two Australian subsets used for the trend analysis. $P_S < 0$ indicates catchments where most precipitation falls in winter and $P_S > 0$ indicates catchments where most precipitation falls in summer. Note that there is some overlap for the two Australian P_S distributions due to the use of KDE.

Table S1: Absolute and relative trends of streamflow sensitivities. Relative trends are normalised with the value from the first year. Note that all relative trends indicate a decrease in magnitude, but are reported as positive numbers for the sake of simplicity.

	Empirical [-/50y]	Analytical [-/50y]	Empirical [%/50y]	Analytical [%/50y]
Germany				
s_P	-0.16	-0.04	26	5
s_{Ep}	+0.16	+0.06	70	11
Australia (most *P* in winter)				
s_P	-0.18	-0.09	40	18
s_{Ep}	+0.11	+0.08	49	26
Australia (most *P* in summer)				
s_P	-0.11	-0.03	15	8
s_{Ep}	+0.04	+0.03	15	15